Nat. Hazards Earth Syst. Sci. Discuss., 1, 4287–4304, 2013
www.nat-hazards-earth-syst-sci-discuss.net/1/4287/2013/
doi:10.5194/nhessd-1-4287-2013

Natural Hazards and Earth System Sciences
Open Access
Discussions

Source model of 18 September 2004 Huntoon Valley earthquake estimated from InSAR

W. J. Lee[1], Z. Lu[2], H. S. Jung[1], and L. Y. Ji[3]

[1]Department of Geoinformatics, The University of Seoul, 163 Siripdaero, Dongdaemun-gu, Seoul, 130-743, Korea
[2]US Geological Survey, Cascades Volcano Observatory, Vancouver, WA 98683, USA
[3]Second Monitoring Center, China Earthquake Administration, Xi'an, Shaanxi, 710054, China

Received: 5 June 2013 – Accepted: 28 July 2013 – Published: 30 August 2013

Correspondence to: Z. Lu (lu@usgs.gov)

Published by Copernicus Publications on behalf of the European Geosciences Union.

Abstract

On 18 September 2004, an $M_w = 5.5$ earthquake struck the Huntoon Valley, California, USA. To measure the coseismic deformation field, we applied interferometric synthetic aperture radar (SAR) (InSAR) technique on ascending and descending SAR images from the ENVISAT satellite. Multi-temporal InSAR images were stacked to reduce the atmospheric artifact and other noise. Deformation signals are obvious across the northeast-trending, left-lateral strike-slip fault that produced the earthquake. Ascending and descending deformation maps allowed us to retrieve the east–west and vertical displacement components. Our results show that the displacement in the east–west component is between −3 and 3 cm while the vertical component is between −1 and 1 cm on both sides of the fault. Modeling the averaged deformation images from both descending and ascending tracks with an elastic dislocation source resulted in a best-fit 8 km-long by 3 km-wide fault model that strikes northeast at a depth of about 4.7 km. The magnitude calculated by InSAR data is $M_w = 5.6$, which is similar to that from the local earthquake catalog and slightly larger than estimates from global earthquake catalogs. Moreover, the InSAR-derived depth is similar to that from the local catalog; both are shallower than those reported in the global catalogs. Our results suggest that the earthquake parameters based on global seismic catalogs can be improved by high-resolution InSAR imagery and modeling.

1 Introduction

The Huntoon Valley is a fault bounded basin within the Excelsior Mountains, California, USA. The valley trends northeast between the Adobe Hills to the southeast and the Excelsior Mountains to the northwest (Wesnousky, 2005) (Fig. 1). There is little sign of recent fault activity other than local occurrences of oversteepening at the base of the range front and a number of well-developed triangular facets on the northwest

NHESSD

1, 4287–4304, 2013

18 September 2004 Huntoon Valley earthquake estimated from InSAR

W. J. Lee et al.

side of the valley (Wesnousky, 2005). Generally, reported slip rate has been less than $0.2\,\mathrm{mm\,yr^{-1}}$ (Adams and Sawyer, 1998).

On 18 September 2004, at 23:02:17 (UTC), an earthquake of $M_w = 5.4$–5.6 occurred just east of Mono Lake and beneath the Adobe Hills of the Huntoon Valley area (Fig. 1) (Table 1). There was no damage reported because this region is unsettled and the event was not so strong. On the other hand, the earthquake produced widely felt shaking in the area from Bridgeport to Bishop, California (USGS LVO, 2005).

Several focal mechanism solutions were released by different organizations using seismic data (Table 1). However, the solutions are slightly different due to possible errors in the velocity model, the poor distribution of seismic stations, and different algorithms for parameter determination (Mellors et al., 2004). Moreover, the use of relative location methods may improve the relative locations, but converting these to the absolute locations usually requires an initial set of known accurate locations, often based on independent measurements (Mellors et al., 2004).

Interferometric synthetic aperture radar (InSAR) utilizes SAR images acquired at different times to derive surface deformation at an unprecedented spatial resolution (e.g., Massonnet and Feigl, 1998; Lu, 2007). The interferometric SAR (InSAR) images can be used to derive source parameters associated with seismic, volcanic and other processes. For earthquake studies, InSAR provides independent information about the earthquake source parameters. This is particularly useful over areas where seismic stations are poorly distributed. Numerous studies have attempted to derive earthquake mechanisms in spite of InSAR limitations such as decorrelation, atmospheric errors and low temporal resolution (e.g., Weston et al., 2011). Furthermore, InSAR images from ascending and descending SAR tracks can be used to calculate the displacement components in the east–west and vertical directions (Wright et al., 2004), which can provide insights into the faulting process without further modeling.

Bell et al. (2008) showed the line-of-sight (LOS) deformation field due to the 19 September 2004 earthquake using only 1 interferogram from a descending track. In this paper, we processed a large number of SAR images from both descending and

NHESSD
1, 4287–4304, 2013

Title Page
Abstract | Introduction
Conclusions | References
Tables | Figures
◀◀ | ▶▶
◀ | ▶
Back | Close
Full Screen / Esc
Printer-friendly Version
Interactive Discussion

ascending tracks. We stacked many interferograms to improve the signal-to-noise ratio of the final deformation images. We derived the deformation field in the east–west and vertical directions using the averaged descending and ascending InSAR images. Finally, we modeled the observed deformation images jointly using an elastic dislocation source and compared the InSAR-derived source parameters with those from various seismic catalogs.

2 Data processing and InSAR results

2.1 Data processing

To measure the coseismic surface deformation, we obtained ascending and descending SAR images from the European Environmental Satellite (Envisat) operating at C-band with a wavelength of 5.6 cm. We used the two-pass InSAR approach (e.g., Massonnet and Feigl, 1998) to form 8 and 5 deformation interferograms with good coherence from one ascending and one descending tracks, respectively. We used a 1-arc-second digital elevation model to correct for the topographic phase contribution in the interferograms. Interferograms were created by using a complex multilook operation with 2 looks in the range and 10 looks in the azimuth directions, resulting in a pixel dimension of about 40 m × 40 m. Inspecting individual interferograms suggested that they are not obviously contaminated by atmospheric artifacts. In order to further reduce atmospheric and other noises, we averaged the 5 interferograms from the descending track (Table 2) and 8 interferograms from the ascending track (Table 3) to generate two averaged deformation images, respectively.

The averaged deformation maps from the ascending and descending tracks then can allow us to retrieve the east–west and vertical displacement components (Wright et al., 2004). Because both the ascending and descending tracks of Envisat are near-polar orbits, we couldn't resolve the deformation field in the north–south direction based on two LOS InSAR observations (Wright et al., 2004; Jung et al., 2011). Let $\boldsymbol{d} = (d_x, d_y)^T$ be the 2-dimensional deformation vector in a local (east, up) reference

NHESSD
1, 4287–4304, 2013

18 September 2004 Huntoon Valley earthquake estimated from InSAR

W. J. Lee et al.

frame. If $\boldsymbol{u}$ is the LOS deformation vector in the same local reference frame, then $\boldsymbol{u}$ is $(\sin\theta\cos\varphi, \cos\theta)^T$, where θ is the radar incidence angle from the vertical and φ is the satellite track angle from north, respectively. If we produce InSAR interferograms (observations) from both descending and ascending tracks, we can obtain the deformation vector $\boldsymbol{d} = -(\boldsymbol{u}^T\boldsymbol{u})^{-1}(\boldsymbol{u}^T\boldsymbol{r})$, where $\boldsymbol{u}$ and $\boldsymbol{r}$ are given by $\boldsymbol{u} = (u_{\mathrm{asc}}, u_{\mathrm{dsc}})^T$ and $\boldsymbol{r} = (r_{\mathrm{asc}}, r_{\mathrm{dsc}})^T$, respectively.

2.2 InSAR results

Averaged interferograms from both descending and ascending tracks are shown in Fig. 2a and b, respectively. The deformation signals are visible across the northeast-trending fault that produced the earthquake. The deformation reached about 2 cm in LOS on both sides of the fault. The east–west and vertical displacement components based on the averaged deformation images from the descending and ascending tracks are shown in Fig. 2c and d, respectively. Figure 3 shows the horizontal and vertical displacements along the profile AB labeled in Fig. 2. The displacement in the east–west component is between −3 cm and 3 cm on both sides of the fault. Meanwhile, the deformation of the vertical component is between −1 cm and 1 cm on both sides of the fault. From the analysis of the profile we can conclude that the horizontal component dominated the deformation pattern.

3 Modelling and analysis

3.1 InSAR deformation modelling

To reveal the focal mechanism parameters of the 18 September 2004 earthquake, we jointly modeled the averaged interferograms from ascending and descending tracks using an elastic dislocation source (Okada, 1985). The rectangular elastic dislocation source consists of 10 model parameters: two location coordinates for the center of source (x, y), depth (z), length, width, three components of slip (strike, dip, tensile),

NHESSD
1, 4287–4304, 2013

and strike and dip of the dislocation plane. We used the downhill simplex method and Monte Carlo simulations (Press et al., 1992) to estimate optimal parameters and their uncertainties, and the root mean square errors between the observed and modeled interferograms as the prediction-fit criterion. The best-fit parameters are listed in Table 4. Figure 4 shows the observed (Fig. 4a and d), modeled (Fig. 4b and e), and residual (Fig. 4c and f) interferograms from descending and ascending tracks, respectively. The modeled interferograms fit the observed interferograms reasonably well. The best-fit fault model strikes approximately N–E with a length of about 8 km and a width of 3 km centered at a depth of 4.7 km.

3.2 Comparison of source parameters from InSAR and seismology

After we obtained the best-fit parameters for the dislocation source, we calculated the earthquake moment magnitude (M_w) based on the formula by Hanks and Kanamori (1979): $M_w = 2/3\log_{10}(M_0) - 10.7$. The seismic moment, M_0, is equal to μAS (Table 4), where μ is the shear strength of the country rock, about 3×10^{11} dyne cm^{-2} for typical continental crust, A is the area of the fault, and S is the average displacement along the fault plane. The moment magnitude calculated for this earthquake based on InSAR modeling is $M_w = 5.6$.

Next, we compared the InSAR-derived earthquake parameters with those from several existing earthquake catalogs: National Earthquake Information Center Preliminary Determination of Epicenters (PDE), California Integrated Seismic Network (CISN), Global Centroid Moment Tensor (CMT), Double-Difference Earthquake Catalog for Northern California (NCAeeDD) (Waldhauser and Schaff, 2008). Overall, InSAR and seismic data agree well regarding the location, moment magnitude, strike and dip of the earthquake (Tables 1 and 4). The difference in earthquake location is less than 3 km (Tables 1 and 4). The InSAR-derived earthquake magnitude is $M_w = 5.6$. This estimate is the same as that from NCAeqDD catalog, but smaller than those from PDE and CMT (Table 1). The InSAR-derived source depth is about 4.7 km (Table 4), which is slightly shallower than most of estimates from earthquake catalogs (Table 1). This is consistent with a global survey that InSAR-derived depth is generally shallower than the estimates from global seismic catalogs (Weston et al., 2011). However, the depth estimate CMT catalog (12.0 km) represents a significant departure from the other catalogs and the InSAR result, suggesting the depth estimate from the global catalog CMT is probably an outlier (Table 1). The strike of the fault from InSAR is nearly identical to those from PDE and CISN catalogs, all of which are similar to the strike of the mapped faults in the area (Fig. 1). The strike from the CMT catalog (339°) is much different from InSAR and other earthquake catalogs, suggesting CMT's estimate on strike is also a biased one. Based on the above analysis, we believe the quality of source parameters from the CMT catalog for the 18 September 2004 earthquake is poorer than the others.

3.3 Seismicity over Huntoon Valley area

Finally, we investigated the seismicity over the Huntoon Valley area during 1984 and 2010 using NCAeeDD catalog. The minimum magnitude completeness for earthquakes over this area is about 0.8 (Wiemer and Wyss, 2000). Based on the earthquake frequency plot (Fig. 5), the seismicity over the Huntoon Valley fault area has been stable before 2004. The increase of seismicity during 2004–2006 consisted of several moderate-sized earthquakes, including an $M_w = 5.2$, an $M_w = 5.4$ and an $M_w = 5.6$ earthquake (Fig. 5). Therefore, we suspect that the observed InSAR deformation field likely represents the cumulative effect of these events. This explains in part why the InSAR-derived moment magnitude is slightly larger than most of the seismic catalogs.

4 Conclusions

Using both descending and ascending Envisat InSAR images, we investigated the 18 September 2004 earthquake over Huntoon Valley, California. We stacked multi-temporal InSAR images to improve the signal-to-noise ratio of the averaged deformation images. We then used the averaged deformation images from both descending and ascending tracks to retrieve the east–west and vertical displacement components. Our results show the displacement in the east–west component is between −3 and 3 cm on both sides of the fault. The deformation of the vertical component is estimated is between −1 and 1 cm on both sides of the fault.

We applied a dislocation source to jointly model the averaged deformation images from the descending and ascending tracks. The best-fit source model determined by InSAR indicates a northeast-trending, left-lateral strike-slip fault with a length of about 8 km and a width of 3 km centered at a depth of 4.7 km. The InSAR-derived source parameters are comparable with those from seismic catalogs and allowed us to judge biased parameter estimates in the CMT catalog. Since InSAR data have a high spatial resolution and can act as an independent remotely sensed data source, modeling InSAR-derived deformation field can improve fault parameters derived in global catalogs, particularly when the distribution of seismic stations is poor.

Acknowledgements. This research was supported by the National Research Foundation of Korea (NRF) grant funded by the Ministry of Educational Science and Technology of Korea (MEST) and USGS Volcano Hazards Program. ENVISAT SAR data are copyrighted by ESA and were provided by ESA under CAT1-2765.

References

Adams, K. D. and Sawyer, T. L.: Compilers, fault number 1302, Huntoon Valley system, in: Quaternary Fault and Fold Database of the United States, US Geological Survey, available at: http://earthquakes.usgs.gov/hazards/qfaults, last access: 4 June 2013, 1998.

Bell, J. W., Oppliger, G. L., and Katzenstein, K.: InSAR across the sierra Nevada basin and range transition zone, Final Technical Report, available at: http://earthquake.usgs.gov/research/external/reports/06HQGR0037.pdf, last access: 27 July 2013, 2008.

Hanks, T. C. and Kanamori, H.: Moment magnitude scale, J. Geophys. Res., 84, 2348–2350, doi:10.1029/JB084iB05p02348, 1979.

Jung, H. S., Lu, Z., Won, J., Poland, M., and Miklius, A.: Mapping three-dimensional surface deformation by combining multiple aperture interferometry and conventional interferometry:

application to the June 2007 eruption of Kīlauea Volcano, Hawaii, IEEE Geosci. Remote S., 8, 34–38, doi:10.1109/LGRS.2010.2051793, 2011.
Lu, Z.: InSAR imaging of volcanic deformation over cloud-prone areas – Aleutian Islands, Photogramm. Eng. Rem. S., 73, 245–257, 2007.
Manzo, M., Ricciardi, G. P., Casu, F., Ventura, G., Zeni, G., Borgstorm, S., Bernardino, P., Del Gaudio, C., and Lanari, R.: Surface deformation analysis in the Ischia Island (Italy) based on spaceborne radar interferometry, J. Volcanol. Geoth. Res., 151, 399–416, 2006.
Massonnet, D. and Feigl, K.: Radar interferometry and its application to changes in the Earth's surface, Rev. Geophys., 36, 441–500, 1998.
Mellors, R. J., Magistrale, H., Earle, P., and Cogbill, A.: Comparison of four moderate size earthquakes in Southern California using seismology and InSAR, B. Seismol. Soc. Am., 94, 2004–2014, 2004.
Okada, Y.: Surface deformation due to shear and tensile faults in a half-space, B. Seismol. Soc. Am., 75, 1135–1154, 1985.
Press, W., Teukolsky, S., Vetterling, W., and Flannery, B.: Numerical Recipes in C, the Art of Scientific Computing, Cambridge Univ. Press, New York, 994 pp., 1992.
US Geological Survey – Long Valley Observatory: Long Valley Observatory Quarterly Report, October–December 2004 and Annual Summary for 2004, available at: http://lvo.wr.usgs.gov/, last access: 15 January 2013, 2005.
Waldhauser, F. and Schaff, D. P.: Large-scale relocation of two decades of Northern California seismicity using cross-correlation and double-difference methods, J. Geophys. Res., 113, B08311, doi:10.1029/2007JB005479, 2008.
Wesnousky, S. G.: Active faulting in the Walker Lane, Tectonics, 24, TC3009, doi:10.1029/2004TC001645, 2005.
Weston, J., Ferreira, A. M. G., and Funning, G. J.: Global compilation of interferometric synthetic aperture radar earthquake source models: 1. comparisons with seismic catalogs, J. Geophys, Res., 116, B08408, doi:10.1029/2010JB008131, 2011.
Wiemer, S. and Wyss, M.: Minimum magnitude of completeness in earthquake catalogs: examples from Alaska, the Western United States, and Japan, B. Seismol. Soc. Am., 90, 859–869, 2000.
Wright, T. J., Parsons, B. E., and Lu, Z.: Toward mapping surface deformation in three dimensions using InSAR, Geophys. Res. Lett., 31, L01607, doi:10.1029/2003GL018827, 2004.

NHESSD
1, 4287–4304, 2013

18 September 2004 Huntoon Valley earthquake estimated from InSAR

W. J. Lee et al.

Table 1. Summary of source parameters for the 18 September 2004 earthquake from four catalogs: PDE, CISN, CMT, NCAeqDD.

Source	Latitude (°)	Longitude (°)	Depth (km)	M_w	Strike (°)	Dip (°)
PDE	38.004	−118.677	5.0	5.4	239	89
CISN	38.009	−118.679	7.6	5.5	239	89
CMT	38.020	−118.690	12.0	5.4	339	76
NCAeqDD	38.0119	118.69099	3.2	5.6	–	–

Note: PDE and CMT are global catalogs whereas CISN and NCAeqDD are local catalogs.

Table 2. ENVISAT SAR interferograms (track no. 485, descending).

No.	Master Date	Slave Date	Bperp [m]	Btemp [day]
1	19 Oct 2003	10 Jul 2005	50	630
2	20 Jun 2004	3 Oct 2004	−5	105
3	20 Jun 2004	14 Aug 2005	−29	420
4	29 Aug 2004	3 Oct 2004	−248	35
5	29 Aug 2004	14 Aug 2005	−272	350

NHESSD
1, 4287–4304, 2013

NHESSD
1, 4287–4304, 2013

18 September 2004 Huntoon Valley earthquake estimated from InSAR

W. J. Lee et al.

Table 3. ENVISAT SAR interferograms (track no. 120, ascending).

No.	Master Date	Slave Date	Bperp [m]	Btemp [day]
1	29 Oct 2003	20 Jul 2005	−189	630
2	29 Oct 2003	3 Oct 2007	82	1435
3	29 Oct 2003	17 Sep 2008	4	1785
4	30 Jun 2004	31 May 2006	54	700
5	8 Sep 2004	3 Oct 2007	−95	1120
6	8 Sep 2004	7 Nov 2007	94	1155
7	8 Sep 2004	9 Jul 2008	−55	1400
8	8 Sep 2004	17 Sep 2008	−174	1470

Table 4. Parameters for the best-fitting dislocation model.

Latitude (°)	Longitude (°)	Depth (km)	Strike (°)	Dip (°)	Length (km)	Width (km)	Strike-slip (mm)	Dip-slip (mm)	Tensile-slip (mm)
38.0258	118.6661	4.7	229	82.7	8.0	3.1	322	16	0

NHESSD

1, 4287–4304, 2013

18 September 2004 Huntoon Valley earthquake estimated from InSAR

W. J. Lee et al.

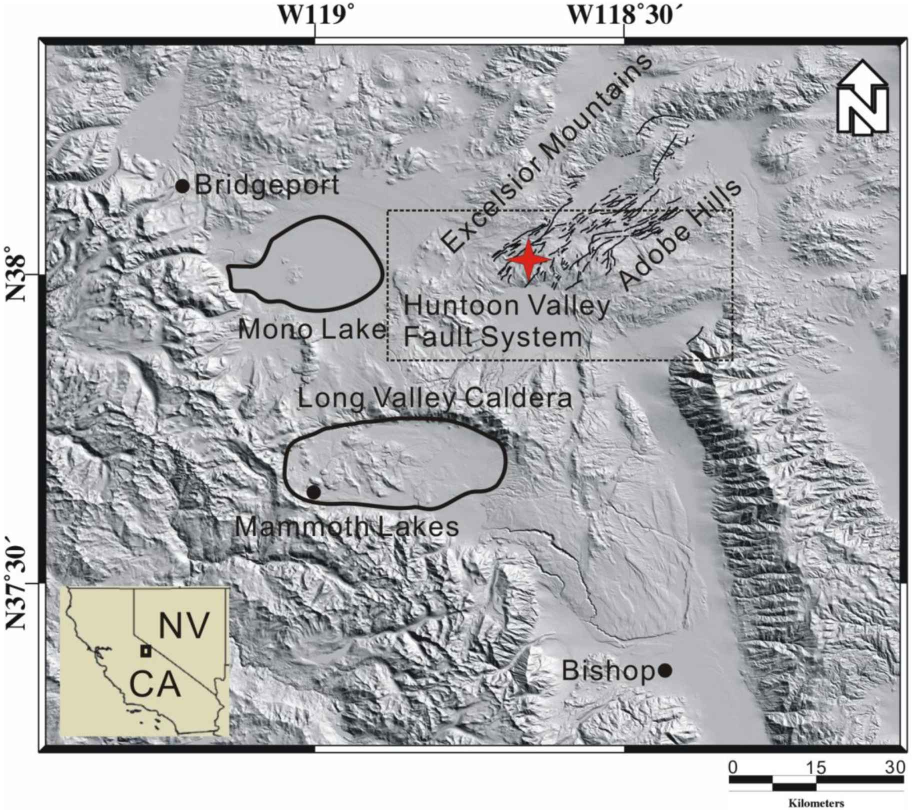

Fig. 1. Shaded relief map of Huntoon Valley and surroundings. Primary geographic features in the region are labeled. Quaternary faults over Huntoon Valley are shown by black lines inside the dashed box. Red star represents the earthquake of $M_w + 5.5$ on 18 September 2004.

NHESSD
1, 4287–4304, 2013

18 September 2004 Huntoon Valley earthquake estimated from InSAR

W. J. Lee et al.

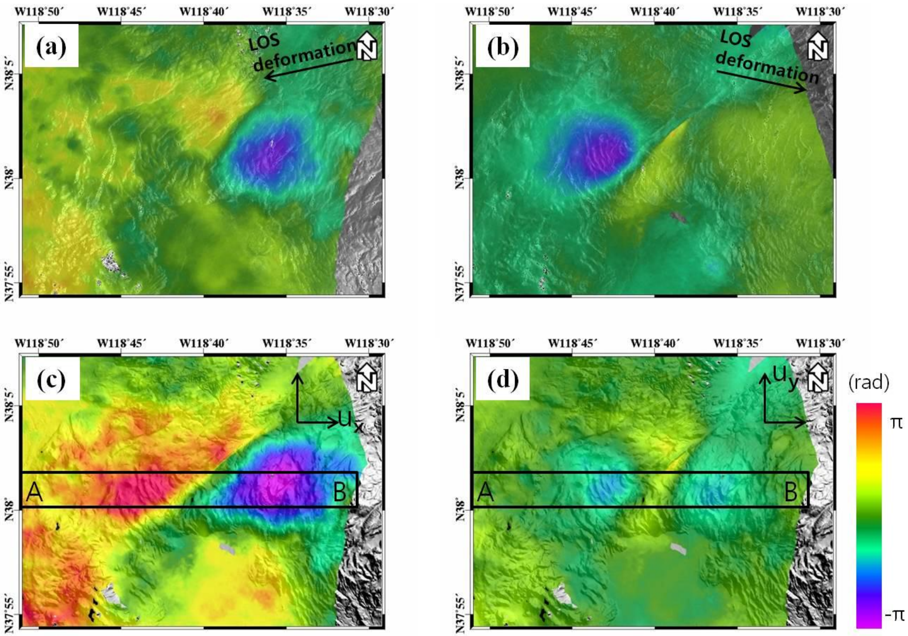

Fig. 2. **(a)** LOS deformation image acquired from a descending track. **(b)** LOS deformation image acquired from an ascending track. **(c)** East–west component of the deformation field. **(d)** Vertical component of the deformation field.

NHESSD
1, 4287–4304, 2013

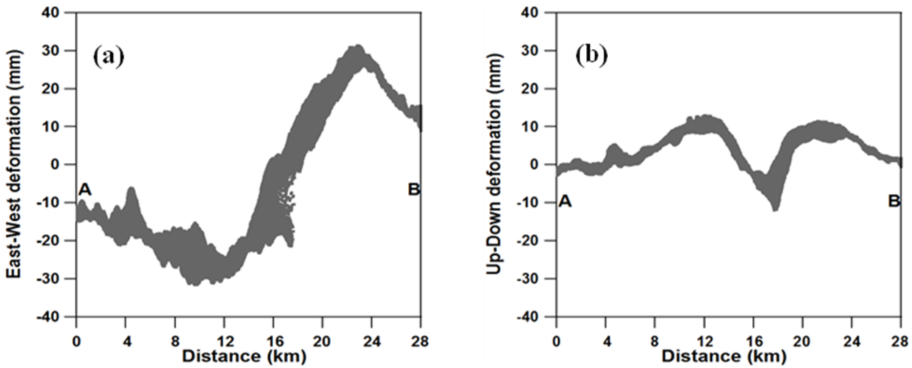

Fig. 3. (a) East–west deformation along a profile AB labeled in Fig. 2c. **(b)** Vertical deformation along the profile.

NHESSD

1, 4287–4304, 2013

18 September 2004 Huntoon Valley earthquake estimated from InSAR

W. J. Lee et al.

Title Page
Abstract | Introduction
Conclusions | References
Tables | Figures
◀| |▶
◀ ▶
Back | Close
Full Screen / Esc
Printer-friendly Version
Interactive Discussion

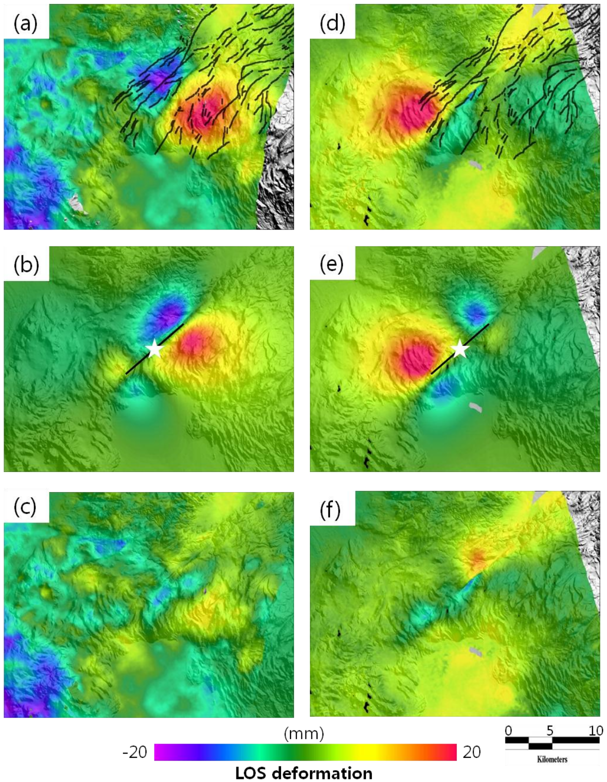

Fig. 4. Observed deformation images from **(a)** descending track and **(d)** ascending track. **(b, e)** Synthetic inteferograms for the descending and ascending track geometries based on the best-fit source model. **(c, f)** Residual interferograms from the descending and ascending tracks, showing the difference between observed and modeled interferograms. White star represents the center of the best-fit earthquake source while the solid line represents the projection of the modeled fault that caused the 18 September 2004 earthquake.

NHESSD
1, 4287–4304, 2013

18 September 2004 Huntoon Valley earthquake estimated from InSAR

W. J. Lee et al.

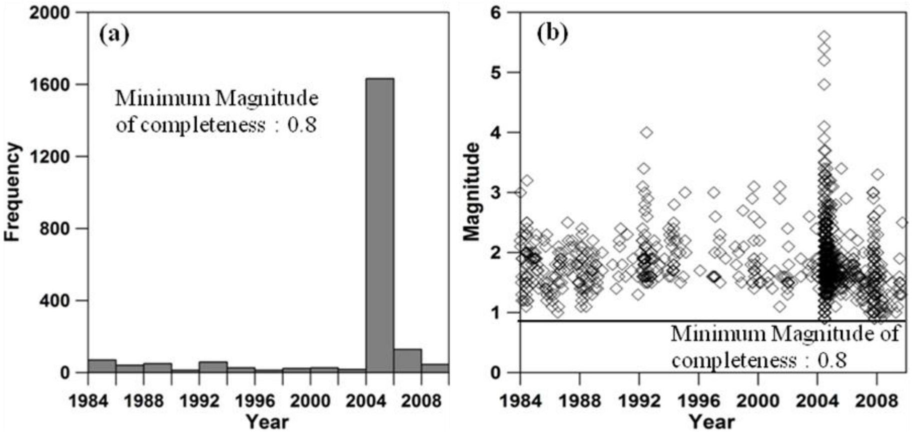

Fig. 5. Distribution of **(a)** frequency and **(b)** magnitude of earthquakes occurred near the Huntoon Valley area from NCAeqDD catalog.

NHESSD
1, 4287–4304, 2013

18 September 2004 Huntoon Valley earthquake estimated from InSAR

W. J. Lee et al.